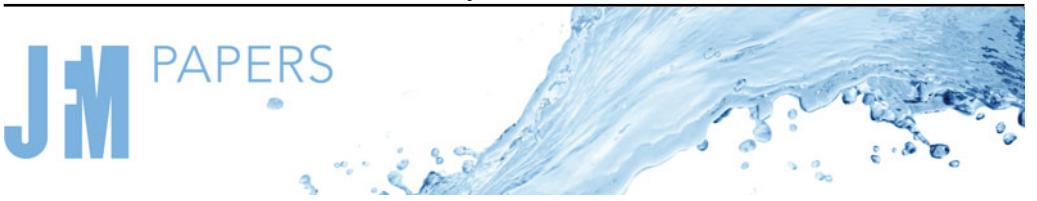
J. Fluid Mech. (2025), *vol.* 1025, A25, doi:10.1017/jfm.2025.10966



On the subcritical transitional threshold in two-dimensional plane Poiseuille flow

Yuanyuan Gao[1], **Tongsheng Wang**[1], **Jianan Chen**[1], **Guang Xi**[1] **and Zhu Huang**[1]

[1]Department of Fluid Machinery and Engineering, Xi'an Jiaotong University, Shaanxi 710049, PR China

Corresponding author: Zhu Huang, zhuhuang@xjtu.edu.cn

(Received 25 March 2025; revised 10 October 2025; accepted 17 November 2025)

The nonlinear Tollmien–Schlichting waves mechanism of subcritical transitional flow in quasi-two-dimensional flow and two-dimensional (2-D) plane Poiseuille flow have been investigated (Camobreco *et al.* 2023 *J. Fluid Mech.*, vol. 963, p. R2; Huang *et al.* 2024 *J. Fluid Mech.*, vol. 994, p. A6). However, the subcritical transitional flow threshold has remained unsolved for 2-D shear flows since the problem was proposed in Trefethen *et al.* (1993 *Science* vol. 261, no. 5121, pp. 578–584). In this study, we proposed a theoretical analysis based on the nonlinear non-modal analysis and asymptotic analysis to quantify the scaling law for subcritical transitional flow of 2-D plane Poiseuille flow. The subcritical transitional flow induced by the critical disturbance experiences the nonlinear edge state with invariant disturbance kinetic energy (Huang *et al.* 2024 *J. Fluid Mech.* vol. 994, p. A6). Consequently, the required magnitude along with the edge state is predicted by asymptotic analysis, and the *a priori* threshold is achieved theoretically. All stages are validated by the numerical minimal seeds of different channels. The proposed theory predicts that the scaling laws are $O(Re^{-11/3})$ and $O(Re^{-7/3})$ for the critical disturbances and their edge state, respectively. While the numerical thresholds of the subcritical transitional flow are $Re^{-11/3\pm0.06}$ and $Re^{-7/3\pm0.05}$, respectively.

Key words: nonlinear instability, transition to turbulence, shear-flow instability

1. Introduction

Despite turbulence being ubiquitous and widely observed from the natural environment to engineering technology, the origin of turbulence has not been well understood since the Reynolds experiment (Reynolds 1883). The linear stability analysis based on linearized Navier–Stokes (NS) equations (Orr 1907) and unstable disturbances has been developed to explain the flow instability of shear flows, which has been recognized as the fundamental

© The Author(s), 2025. Published by Cambridge University Press.

https://doi.org/10.1017/jfm.2025.10966 Published online by Cambridge University Press

stage in flow transition to turbulence. However, the onset of turbulence continues to be a persistent focal point of research (see Avila *et al.* 2011; Barkley *et al.* 2015). Among the notable research contributions, the critical Reynolds number has been precisely determined by applying rigorous asymptotic analysis (Lin 1944). Nonetheless, turbulence can originate and evolve subcritically in the absence of linear unstable disturbances (Orszag & Patera 1980). For example, the plane Poiseuille flow demonstrates instability when the Reynolds number exceeds the critical value of 5772.2 (Orszag 1971); however, sustained turbulence could be observed experimentally (Lemoult, Aider & Wesfreid 2012) and numerically (Farano *et al.* 2015) when the Reynolds number is less than 5000.

The non-normality of the linearized NS operator (Trefethen *et al.* 1993) predicts adequate transient growth of appropriate disturbances *a priori* to their exponential decay in linearly stable flows (see Gustavsson 1991; Schmid 2007). The amplified finite-amplitude disturbance is subject to potential nonlinear interactions and secondary linear instabilities, thereby contributing to the subcritical transition to turbulence (Reddy *et al.* 1998). Transient growth based on direct numerical simulations (DNS) provides schematic and qualitative scenarios in the subcritical transition to turbulence. Therefore, the transition thresholds in the three-dimensional (3-D) channel flows could be calculated (see Reddy *et al.* 1998; Trefethen *et al.* 2000; Duguet, Brandt & Larsson 2010), and the threshold could be affected by the numerical resolution (Duguet *et al.* 2010) . However, the subcritical transition to turbulence is essentially a very strong nonlinear dynamic process (Hof *et al.* 2004). Furthermore, nonlinearity substantially enhances the transient growth observed in shear flows (see Pringle & Kerswell 2010; Huang & Hack 2020) and provides spatially localized flow structures that represent optimal disturbances. Actually, the localized structures play a crucial role in the subcritical transition to turbulence in 3-D plane shear flows. Localized turbulent puffs and slugs in pipe flow have been investigated for subcritical dynamics (Nishi *et al.* 2008; Willis & Kerswell 2009), while turbulent bands and stripes are found in plane Couette and Poiseuille flows with remarkable channel length and width (Parente *et al.* 2022; Marensi, Yalniz & Hof 2023). Nonlinear non-modal stability analysis captures spatially localized disturbances in a relatively smaller computational domain that trigger the subcritical transition to turbulence via an edge state with streamwise streaks in pipe and plane channel flow (Rabin, Caulfield & Kerswell 2012; Kerswell 2018).

A minuscule initial perturbation can lead to markedly different final states after sufficiently long strong nonlinear interactions in the nonlinear dynamic system. Consequently, the nonlinear interacted edge state wrapped in the laminar–turbulent boundary illustrates and approximates the most dangerous subcritical transition to turbulence (Kerswell 2018). To touch on the edge state, optimization methodologies have been employed to identify disturbances of minimal energy as governed by the full NS equations based on DNS. The minimal energy disturbance undergoes a rapid nonlinear transient amplification, reaching the edge state with an adequately extended duration, preceding the onset of the turbulent state. The nonlinear non-modal stability analysis has achieved great numerical success in the most dangerous subcritical transition for the pipe flow (Pringle, Willis & Kerswell 2012) and the plane Couette flow (Monokrousos *et al.* 2011). Moreover, the nonlinear variational optimization could identify minimal seeds (Rabin *et al.* 2012; Duguet *et al.* 2013) and minimal energy thresholds for sustained turbulent bands (Parente *et al.* 2022) in plane channel flows. For 3-D plane Couette flow, the transition thresholds for the localized nonlinear optimal disturbance with scaling $Re^{-2.7}$ are much smaller than those of the linear optimal disturbance with scaling $Re^{-2.0}$ (Duguet *et al.* 2013). Recently, the streamwise localized minimal seeds are also observed

https://doi.org/10.1017/jfm.2025.10966 Published online by Cambridge University Press

in the two-dimensional (2-D) plane Poiseuille flow, and the subcritical transitional flow has been investigated for $Re \leqslant 5000$ (Huang *et al.* 2024).

Evidently, the reliable threshold constitutes the most dangerous subcritical transition to turbulence and holds considerable significance from both fundamental and practical perspectives. The theories of transient growth and nonlinear non-modal instability could summarize numerical thresholds based on DNS. However, the *a posteriori* thresholds might not agree with the *a priori* predictions by theoretical analysis (see Chapman 2002; Duguet *et al.* 2010, 2013; Bedrossian, Germain & Masmoudi 2015). For 3-D plane Couette flow, Chapman (2002) predicts the transition threshold scales with Re as Re^{-2}, while Bedrossian *et al.* (2015) concludes that the threshold is theoretically Re^{-3}. Moreover, the transitional thresholds Re^{-2} and $Re^{-2.7}$ are calculated for the linear and nonlinear optimal disturbances, respectively (Duguet *et al.* 2010, 2013). A mechanism or theoretical framework capable of elucidating or predicting the *a priori* disturbance threshold for subcritical transitional flows, which can be directly validated through flow physics, has yet to be established. Therefore, the establishment of a reliable threshold, substantiated by both the *a priori* theoretical predictions and the *a posteriori* numerical validations, represents an inherent and principal challenge for the theory of subcritical transition. In other words, what is the exact exponent κ if E_c denotes the scaling of the energy threshold with Re as $O(Re^{-\kappa})$ asymptotically (Trefethen *et al.* 1993)? This fundamental problem has persisted as one of the most prominent challenges for the mathematical treatment of the NS equations (Bedrossian *et al.* 2015, 2019; Ding & Lin 2022; Del Zotto 2023) and for the physical understanding of subcritical transitional flows.

To address the challenge posed by the most dangerous subcritical transition to turbulence, this study developed a novel theoretical framework that integrates the principles of linear asymptotic analysis, transient growth and nonlinear non-modal instability analysis, in consideration of the intrinsic nonlinear dynamics of transitional flow. Based on linear instability theory, the 2-D flow is more unstable than the 3-D counterpart for plane shear flows. For the nonlinear non-modal stability analysis, the streamwise localized minimal seeds approach the long-sustained energy-conserved nonlinear edge state before triggering the subcritical transition in the 2-D plane channel flow (Huang *et al.* 2024). The transitional scenarios are very similar to that of 3-D plane Couette flow, including the streamwise localized minimal seed and the energy-conserved nonlinear edge state. Although the Poiseuille flow in the 2-D plane based on 2-D NS equations could not transition to small-scale turbulence (Boffetta & Ecke 2012), the subcritical transition mechanism in the 2-D plane channel flow could offer the main subcritical transition mechanism and the theoretical foundation for 3-D shear flows. Moreover, 2-D plane shear flows could be approximated by external electromagnetic forces (Camobreco *et al.* 2020, 2023). Therefore, the 2-D plane Poiseuille flow is chosen to construct our theoretical framework in this study.

According to Kerswell (2018), the minimal seed triggers the most dangerous subcritical transition. The possible disturbance close to the minimal seed experiences rapid Orr amplification. Then the coherent fluid structures persist along the edge state for a long enough period with fully developed nonlinear interactions. Finally, the unstable manifold is attracted by either the turbulent or laminar attractor, inducing transitional flow or relaminarization, respectively. Based on our previous research (Huang *et al.* 2024), the saturated nonlinear interacted edge state maintains energy conservation and exhibits an energy plateau. Consequently, this provides an opportunity to quantify the disturbance velocities in conjunction with the saturated nonlinear edge state, and the amplitude of the requisite minimal seed can be inferred by incorporating linear Orr amplification.

https://doi.org/10.1017/jfm.2025.10966 Published online by Cambridge University Press

Adhering to this philosophy, the mechanism governing the 2-D subcritical transitional flow in plane Poiseuille flow can be quantitatively characterized once the magnitude of the disturbance along the nonlinear edge state E_{es} is determined. In this study, the *a priori* threshold is predicted through theoretical asymptotic analysis, accomplished by instigating instability within the inner flow via nonlinear interactions, as presented in § 2. *A posteriori*, the theoretical prediction has been validated through the nonlinear minimal seeds derived from nonlinear non-modal analysis and DNS, as shown in § 3. The discussions and conclusions are summarized in § 4.

2. Theoretical analysis

For the Poiseuille flow in the 2-D plane driven by a constant pressure gradient with the base flow $U(y) = (1 - y^2)\boldsymbol{e_x}$, the Reynolds number $Re = U_{max}h/\nu$ where h is the half-depth of the channel. Let the disturbances be $\boldsymbol{u} = \boldsymbol{u}_{tot} - \boldsymbol{U}$, $p = p_{tot} - P$, where $\boldsymbol{u}_{tot}$ and p_{tot} are the total velocity vector and pressure, and U and P are the velocity vector and pressure of the steady state base flow. Therefore, the NS equations are

$$\frac{\partial \boldsymbol{u}}{\partial t} + \boldsymbol{U}\cdot\boldsymbol{\nabla u} + \boldsymbol{u}\cdot\boldsymbol{\nabla U} + \boldsymbol{u}\cdot\boldsymbol{\nabla u} = -\boldsymbol{\nabla} p + \frac{1}{Re}\nabla^2\boldsymbol{u}, \quad \boldsymbol{\nabla}\cdot\boldsymbol{u} = 0. \tag{2.1}$$

Here $\boldsymbol{u}$ is the velocity disturbance vector (u, v), and the imposed conditions are $\boldsymbol{u}(x, \pm 1) = 0$ on the walls. According to (2.1), we can obtain the governing equation of wall-normal velocity v without the pressure gradient

$$\frac{\partial \nabla^2 v}{\partial t} + U\nabla^2 v_x - \frac{\mathrm{d}^2 U}{\mathrm{d}y^2} v_x - \frac{\nabla^4 v}{Re} = \boldsymbol{Non}(v), \quad u_x + v_y = 0, \tag{2.2}$$

where the nonlinear terms $\boldsymbol{Non}(v)$ are

$$\boldsymbol{Non}(v) = v_x(u_{yy} - v_{xy}) + v_y(v_{xx} + v_{yy}) - u(v_{xxx} + v_{xyy}) - v(v_{xxy} + v_{yyy}). \tag{2.3}$$

The nonlinear interactions are evoked after the Orr amplification, and the nonlinear edge state could be reached (Huang *et al.* 2024). For the periodic boundary condition in the streamwise direction, we can decompose the velocity disturbance into Fourier modes. For example,

$$v(x, y, t) = \sum_{n=0}^{N}\sum_{k_t=0}^{N_t}\sum_{k_x=0}^{N_x} \tilde{v}_n(y)\exp^{(-i\omega k_t t + i\alpha k_x x)}, \tag{2.4}$$

where $\tilde{v}_n(y)$ is the nth continuous function in the wall-normal direction y, ω is the frequency and α is the streamwise wavenumber. Here n, k_t and k_x are the summation indices with the truncation order of N, N_k and N_x, respectively. However, wave-like solutions are popular in stability analysis according to previous studies (Schmid & Henningson 2001; Chapman 2002). Therefore, the wave-like solutions are employed in this study,

$$v(x, y, t) = \sum \tilde{v}(y)\exp^{(-i\omega t + i\alpha x)}, \tag{2.5}$$

where $\tilde{v}(y)$ is the continuous function in the wall-normal direction. Then, we can obtain

$$(i\alpha U - i\omega)\left(\frac{\mathrm{d}^2}{\mathrm{d}y^2} - \alpha^2\right)\tilde{v} - i\alpha\frac{\mathrm{d}^2 U}{\mathrm{d}y^2}\tilde{v} - \frac{1}{Re}\left(\frac{\mathrm{d}^2}{\mathrm{d}y^2} - \alpha^2\right)^2\tilde{v} = \boldsymbol{Non}(\tilde{v}), \tag{2.6}$$

$$i\alpha\tilde{u} = -\mathrm{d}\tilde{v}/\mathrm{d}y. \tag{2.7}$$

https://doi.org/10.1017/jfm.2025.10966 Published online by Cambridge University Press

According to the continuity (2.7), the nonlinear terms are approximated as follows:

$$\begin{aligned}\boldsymbol{Non}(v) &= v_x(u_{yy}-v_{xy})+v_y(v_{xx}+v_{yy})-u(v_{xxx}+v_{xyy})-v(v_{xxy}+v_{yyy})\\ &\sim i\alpha\tilde{v}\left(-\frac{1}{i\alpha}\frac{\mathrm{d}^3\tilde{v}}{\mathrm{d}y^3}-i\alpha\frac{\mathrm{d}\tilde{v}}{\mathrm{d}y}\right)+\frac{\mathrm{d}\tilde{v}}{\mathrm{d}y}\left(-\alpha^2\tilde{v}+\frac{\mathrm{d}^2\tilde{v}}{\mathrm{d}y^2}\right)\\ &\quad-\frac{1}{i\alpha}\frac{\mathrm{d}\tilde{v}}{\mathrm{d}y}\left(-i\alpha^3\tilde{v}+i\alpha\frac{\mathrm{d}^2\tilde{v}}{\mathrm{d}y^2}\right)-\tilde{v}\left(i\alpha^2\frac{\mathrm{d}\tilde{v}}{\mathrm{d}y}+\frac{\mathrm{d}^3\tilde{v}}{\mathrm{d}y^3}\right)\\ &\sim\tilde{v}\left(-\frac{\mathrm{d}^3\tilde{v}}{\mathrm{d}y^3}+\alpha^2\frac{\mathrm{d}\tilde{v}}{\mathrm{d}y}\right)+\frac{\mathrm{d}\tilde{v}}{\mathrm{d}y}\left(-\alpha^2\tilde{v}+\frac{\mathrm{d}^2\tilde{v}}{\mathrm{d}y^2}\right)\\ &\quad-\frac{\mathrm{d}\tilde{v}}{\mathrm{d}y}\left(-\alpha^2\tilde{v}+\frac{\mathrm{d}^2\tilde{v}}{\mathrm{d}y^2}\right)-\tilde{v}\left(i\alpha^2\frac{\mathrm{d}\tilde{v}}{\mathrm{d}y}+\frac{\mathrm{d}^3\tilde{v}}{\mathrm{d}y^3}\right).\end{aligned}\tag{2.8}$$

The wall-normal derivative would be more significant near the channel walls for the disturbance of the wall mode (Chapman 2002; Huang *et al.* 2024). Then, the leading terms are $v_x u_{yy}$ and vv_{yyy}, obviously with the same magnitude as $\tilde{v}\mathrm{d}^3\tilde{v}/\mathrm{d}y^3$. Therefore, $\boldsymbol{Non}(\tilde{v})\sim\tilde{v}\mathrm{d}^3\tilde{v}/\mathrm{d}y^3$ is chosen for the following analysis for convenience.

Lin (1944) introduced $(\alpha Re)^{1/3}$ into the linearized NS equations (Orr–Sommerfeld (OS) equations) to study the linear instability analysis; asymptotic analysis was performed and great success was achieved since the critical Reynolds number Re_c is predicted to be approximately 8000 ($Re^{1/3}$ is approximately 20) for the 2-D plane Poiseuille flow. Here $Re_c = 5772.2$ is well known now for the disturbance of wall mode in the 2-D plane Poiseuille flow (Orszag 1971; Schmid & Henningson 2001). Chapman (2002) performed the asymptotic analysis to investigate the subcritical transition in channel flows, mainly focused on the wall and centre modes. Therefore, inspired by the asymptotic analysis (Lin 1944; Chapman 2002), nonlinear disturbances of the wall mode (Huang *et al.* 2024) are considered, and the amplitude required for the nonlinear interaction could be achieved when it is sufficient to induce instability and trigger the subcritical transition. For the plane Poiseuille flow, the Orr amplification of the disturbance occurs near the channel wall due to the notable mean shear, and the nonlinear optimal disturbances are found to be wall modes (Huang *et al.* 2024). Before the nonlinear terms are notable, let us consider the OS equation

$$(i\alpha U-i\omega)\left(\frac{\mathrm{d}^2}{\mathrm{d}y^2}-\alpha^2\right)\tilde{v}-i\alpha\frac{\mathrm{d}^2U}{\mathrm{d}y^2}\tilde{v}-\frac{1}{Re}\left(\frac{\mathrm{d}^2}{\mathrm{d}y^2}-\alpha^2\right)^2\tilde{v}=0.\tag{2.9}$$

Since the wall modes near the channel wall obey the following scalings (Chapman 2002):

$$y=-1+(Re\alpha)^{-1/3}y',\quad \omega/\alpha=\gamma=(Re\alpha)^{-1/3}\gamma'.\tag{2.10}$$

Substituting (2.10) into (2.9), the inner flow near the channel should obey the following equation:

$$\begin{aligned}&\left[i\alpha(1-((Re\alpha)^{-1/3}y'-1)^2)-i\alpha(Re\alpha)^{-1/3}\gamma'\right]\left[(Re\alpha)^{2/3}\frac{\mathrm{d}^2\tilde{v}_i}{\mathrm{d}y'^2}-\alpha^2\tilde{v}_i\right]\\ &\quad+2i\alpha\tilde{v}_i-\frac{1}{Re}\left[(Re\alpha)^{2/3}\frac{\mathrm{d}^2}{\mathrm{d}y'^2}-\alpha^2\right]^2\tilde{v}_i=0,\end{aligned}\tag{2.11}$$

https://doi.org/10.1017/jfm.2025.10966 Published online by Cambridge University Press

which is

$$(Re\alpha)^{1/3}\left[i(2y'-\gamma')\frac{\mathrm{d}^2\tilde{v}_i}{\mathrm{d}y'^2}-\frac{\mathrm{d}^4\tilde{v}_i}{\mathrm{d}y'^4}\right]+2i\tilde{v}_i-iy'^2\frac{\mathrm{d}^2\tilde{v}_i}{\mathrm{d}y'^2}$$
$$+(Re\alpha)^{-1/3}\left[2\alpha^2\frac{\mathrm{d}^2\tilde{v}_i}{\mathrm{d}y'^2}-i(2y'-\gamma')\alpha^2\tilde{v}_i\right]+(Re\alpha)^{-2/3}y'^2\alpha^2\tilde{v}_i-\frac{\alpha^4\tilde{v}_i}{Re\alpha}=0. \quad (2.12)$$

Therefore, the leading equation for the inner flow near the channel wall is

$$(Re\alpha)^{1/3}\left[i(2y'-\gamma')\frac{\mathrm{d}^2\tilde{v}_i}{\mathrm{d}y'^2}-\frac{\mathrm{d}^4\tilde{v}_i}{\mathrm{d}y'^4}\right]=0, \quad (2.13)$$

with boundary conditions $\tilde{v}_i=\mathrm{d}\tilde{v}_i/\mathrm{d}y=0$ on the wall $y=-1$ or $y'=0$. If the coefficient $(Re\alpha)^{1/3}$ is not zero, the following equation is obtained:

$$i(\gamma'-2y')\frac{\mathrm{d}^2\tilde{v}_i}{\mathrm{d}y'^2}+\frac{\mathrm{d}^4\tilde{v}_i}{\mathrm{d}y'^4}=0, \quad (2.14)$$

which is the same as the (5.35) in Chapman (2002). Consequently, according to the rigorous asymptotic analysis in §§ 4 and 5 of Chapman (2002), the left-hand terms of (2.6) should be approximately $(\alpha Re)^{1/3}\tilde{v}_i$ near the channel wall. Next, we should focus on the amplitude of the leading nonlinear terms on the right-hand side of (2.6).

The inner solution has the form of the Airy function for the leading terms, according to (Lin 1944)

$$\frac{\mathrm{d}^2\tilde{v}_i}{\mathrm{d}y'^2}\sim\mathrm{Airy}\left[(2y'-\gamma')i^{1/3}\right],\quad \frac{\mathrm{d}^4\tilde{v}_i}{\mathrm{d}y'^4}\sim(2y'-\gamma')\mathrm{Airy}\left[(2y'-\gamma')i^{1/3}\right]. \quad (2.15)$$

In other words,

$$\frac{\mathrm{d}^4\tilde{v}_i}{\mathrm{d}y'^4}\sim(2y'-\gamma')\frac{\mathrm{d}^2\tilde{v}_i}{\mathrm{d}y'^2}. \quad (2.16)$$

It is straightforward to obtain

$$\frac{\mathrm{d}^2\tilde{v}_i}{\mathrm{d}y'^2}\sim(2y'-\gamma')\tilde{v}_i,\quad \frac{\mathrm{d}^3\tilde{v}_i}{\mathrm{d}y'^3}\sim(2y'-\gamma')^{3/2}\tilde{v}_i,\quad \text{and}\quad \frac{\mathrm{d}^4\tilde{v}_i}{\mathrm{d}y'^4}\sim(2y'-\gamma')^2\tilde{v}_i. \quad (2.17)$$

For the outer solution, the unsteady and diffusive terms are usually omitted (Chapman 2002) to obtain the inviscid flow equation. Then, (2.9) could be simplified as follows:

$$(i\alpha U)\left(\frac{\mathrm{d}^2}{\mathrm{d}y^2}-\alpha^2\right)\tilde{v}_o-i\alpha\frac{\mathrm{d}^2U}{\mathrm{d}y^2}\tilde{v}_o=0. \quad (2.18)$$

Therefore, the outer inviscid flow could be obtained by solving the equation

$$(1-y^2)\left(\frac{\mathrm{d}^2}{\mathrm{d}y^2}-\alpha^2\right)\tilde{v}_o+2\tilde{v}_o=0. \quad (2.19)$$

The outer flow solution has the following form:

$$\tilde{v}_o\sim c_1[1+(1+y)\log(1+y)]+c_2\left[(1+y)+0.5(1+y)^2+\dots\right], \quad (2.20)$$

with two certain non-zero coefficients (Chapman 2002). It implies that the inner limit of the outer solution has the following estimations $\tilde{v}_o\sim c_1$ and $\mathrm{d}\tilde{v}_o/\mathrm{d}y\sim c_1+c_2$ as y tends to -1, which offers the boundary condition approximation for the outer limit of the inner solution.

https://doi.org/10.1017/jfm.2025.10966 Published online by Cambridge University Press

According to nonlinear non-modal analysis (Kerswell 2018), the nonlinear energy-conserved edge state is approached with a sufficiently long time period. Moreover, the subcritical transition is triggered by the optimal disturbance with an energy slightly larger than the critical energy (Rabin *et al.* 2012; Kerswell 2018; Huang *et al.* 2024). Consequently, the subcritical transition processes could be treated as two main stages including the Orr amplification and the evoked nonlinear interactions for 2-D plane Poiseuille flow, because the triggered subcritical transition after the nonlinear edge state is easily achieved by increasing the critical energy slightly. Therefore, if the required magnitude of the nonlinear edge state could be quantified, the transition thresholds might be estimated with the transient growth of Re^2. For the sustained nonlinear edge state, the left-hand leading term of (2.6) should be balanced by the leading nonlinear term to induce instability. In this study, we assumed that the two terms are balanced near the matched boundary, which has not been investigated before. For the inner flow, all the terms on the left-hand side are considered and are of the order of $(Re\alpha)^{1/3}\tilde{v}_i$ after the Orr amplification according to (2.14) (Chapman 2002). While for the outer flow, the leading nonlinear term on the right-hand side is dominated by $\tilde{v}_o \mathrm{d}^3\tilde{v}_o/\mathrm{d}y^3$. Near the matched boundary, i.e. the innermost of the outer solution, the solution is assumed to be sufficiently continuous, which is physically reasonable, then $\tilde{v}_o \sim \tilde{v}_i$ and $\mathrm{d}^3\tilde{v}_o/\mathrm{d}y^3 \sim \mathrm{d}^3\tilde{v}_i/\mathrm{d}y^3$. Based on the scaling (2.10) in the inner solution region, we can obtain

$$\tilde{v}_o\frac{\mathrm{d}^3\tilde{v}_o}{\mathrm{d}y^3} \sim \tilde{v}_o\frac{\mathrm{d}^3\tilde{v}_i}{\mathrm{d}y^3} = \tilde{v}_o\left[(Re\alpha)^{1/3}\right]^3\frac{\mathrm{d}^3\tilde{v}_i}{\mathrm{d}y'^3} = (Re\alpha)\tilde{v}_o\frac{\mathrm{d}^3\tilde{v}_i}{\mathrm{d}y'^3}. \tag{2.21}$$

Since the inner solution has the form of the Airy function as shown in (2.17), we can obtain

$$\frac{\mathrm{d}^3\tilde{v}_i}{\mathrm{d}y'^3} \sim (2y'-\gamma')^{3/2}\tilde{v}_i = \left[(2+2y-\gamma)(Re\alpha)^{1/3}\right]^{3/2}\tilde{v}_i. \tag{2.22}$$

Hence, the magnitude of the term could be estimated as

$$\frac{\mathrm{d}^3\tilde{v}_i}{\mathrm{d}y'^3} \sim (Re\alpha)^{1/2}\tilde{v}_i, \tag{2.23}$$

if only the leading terms are considered. Therefore, we can obtain the magnitude of the leading nonlinear term near the matched boundary

$$\tilde{v}_o\frac{\mathrm{d}^3\tilde{v}_o}{\mathrm{d}y^3} \sim (Re\alpha)\tilde{v}_o\frac{\mathrm{d}^3\tilde{v}_i}{\mathrm{d}y'^3} \sim (Re\alpha)^{3/2}\tilde{v}_o\tilde{v}_i. \tag{2.24}$$

Consequently, $(Re\alpha)^{3/2}\tilde{v}_o\tilde{v}_i$ should be balanced by the left-hand term $(Re\alpha)^{1/3}\tilde{v}_i$ to maintain the nonlinear edge state and induce instability to the inner solution near the outer limit of the inner solution. That is to say,

$$(Re\alpha)^{1/3}\tilde{v}_i \sim (Re\alpha)^{3/2}\tilde{v}_o\tilde{v}_i,\ \ \tilde{v}_o \sim (Re\alpha)^{-7/6}. \tag{2.25}$$

It is noteworthy that the leading nonlinear term is caused by the mutual nonlinear interactions between u and v. This implies that the perturbation magnitudes of both u and v are approximate $(Re\alpha)^{-7/6}$ along the edge state to trigger the subcritical transitional flow. Recall that the $O(Re\alpha)$ amplification of velocity v by the Orr mechanism according to (2.9) before nonlinear interactions are evoked. Consequently, the optimal initial perturbation of wall mode for velocity v is required to be $(Re\alpha)^{-13/6}$ in order to facilitate the onset of subcritical transitional flow. As concluded in the previous study (Huang *et al.* 2024), the nonlinear optimal disturbances manifest as wall modes, with the

https://doi.org/10.1017/jfm.2025.10966 Published online by Cambridge University Press

initial kinetic energy of disturbance u being approximately $(Re\alpha)^{2/3}$ times greater than that of v, i.e. $E_{u0} \sim (Re\alpha)^{2/3} E_{v0}$. That is to say, the scaling law of the transition threshold is dominated by the velocity perturbation u and should be around $(Re\alpha)^{-11/3}$ for the subcritical transitional flow in the 2-D plane Poiseuille flow.

In summary, the subcritical transitional thresholds in the 2-D plane Poiseuille flow are as follows. For minimal seeds, $E_{vms} \sim (Re\alpha)^{-13/3}$ and $E_{ums} \sim (Re\alpha)^{-11/3}$, this consequently leads to $E_{0ms} = (E_{ums} + E_{vms}) \sim (Re\alpha)^{-11/3}$. The disturbance energy required along the saturated nonlinear interacted edge state is $E_{ues} \sim E_{ves} \sim (Re\alpha)^{-7/3}$. The theoretical predictions are consistent with the conjecture (see Trefethen *et al.* 1993) since $\kappa = 11/3 > 2$.

3. Numerical experiments and results

The 2-D turbulent flow is strictly limited in laboratory or nature (Boffetta & Ecke 2012; Sulpizio *et al.* 2019), therefore, numerical experiments based on DNS are the reasonable choice. To capture the subcritical transition experiencing the edge state, the disturbance energy density is defined as

$$E(t) = \frac{1}{2A} \int_A \left[u^2(t) + v^2(t)\right] \mathrm{d}A \tag{3.1}$$

where A is the area of the 2-D channel. The energy densities associated with disturbances in the streamwise and vertical velocity components are

$$E_u(t) = \frac{1}{2A} \int_A u^2(t)\, \mathrm{d}A, \quad E_v(t) = \frac{1}{2A} \int_A v^2(t)\, \mathrm{d}A. \tag{3.2}$$

Nonlinear optimizations are performed using the well-developed direct-adjoint looping method (Pringle & Kerswell 2010) based on Diablo DNS codes (Taylor 2008). The energy gain of the disturbance is chosen as the objective function (Rabin *et al.* 2012), and convergence is obtained when the variation of the energy gain between two successive iterations is smaller than 1×10^{-6}. To identify the minimal seed, the disturbance energy bisection technique is used (Rabin *et al.* 2012; Huang *et al.* 2024). Firstly, the optimization is performed with the random initial disturbance of a sufficiently large initial disturbance energy to achieve subcritical transitional flow with target time T. Then, the computed disturbance rescaled with a much smaller initial energy is used as the initial guess for the optimization to obtain the relaminarization. Consequently, the disturbance energy is bisected to repeat the optimization to obtain the nonlinear edge state and the numerical transition threshold. To observe saturated nonlinear interactions of the edge state, the target times are $T = 1000$ for $Lx = 8\pi$ and $T = 2000$ for $Lx = 20\pi$, respectively, based on the previous study (Huang *et al.* 2024).

According to previous studies (Jiménez 1990; Huang *et al.* 2024), long channels with lengths $Lx = 8\pi$ and 20π with grid resolutions 512×512 and 1024×512, respectively, are considered in the present study based on grid independence tests in Huang *et al.* (2024). Furthermore, to avoid the effects of numerical resolutions on the transition thresholds at high Reynolds numbers (Duguet *et al.* 2010), double grid resolutions 1024×1024 and 2048×1024 are considered for $Lx = 8\pi$ and 20π, respectively, and the difference is less than one per cent at $Re = 5400$. Due to 2-D nonlinear travelling wave effects on the plane Poiseuille flow, subcritical transition states could be identified at $Re = 2939$ (Hagan & Priede 2015). Therefore, the range from 2950 to 5400 is focused on verifying the theory of asymptotic analysis.

https://doi.org/10.1017/jfm.2025.10966 Published online by Cambridge University Press

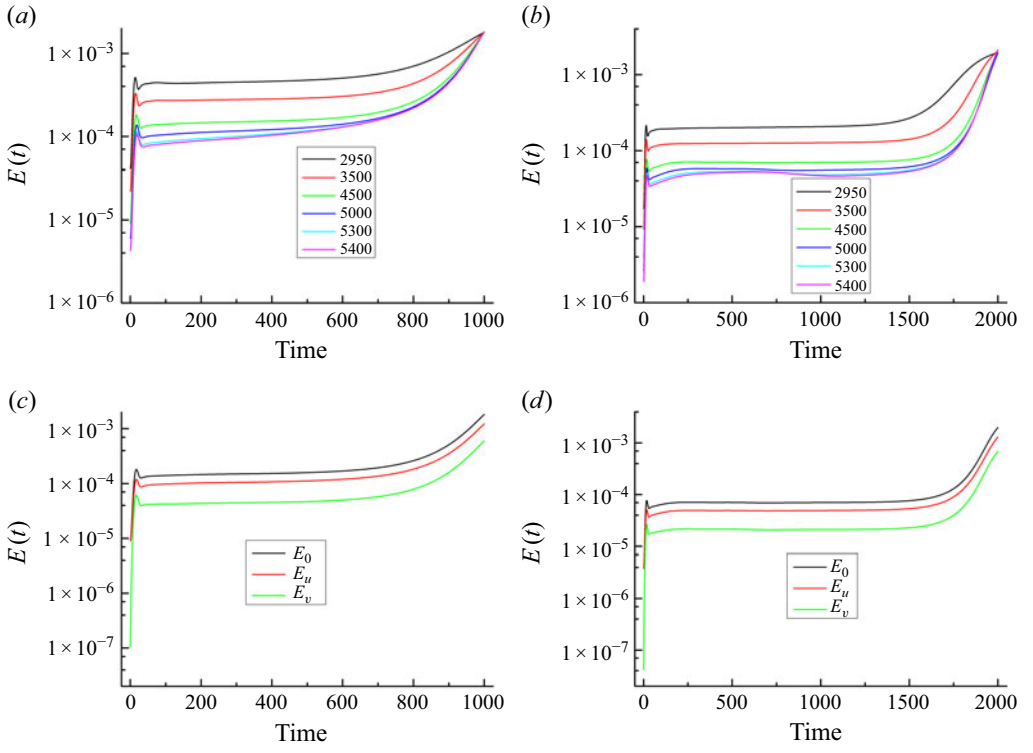


Figure 1. Time evolution of energy densities of minimal seed at different Re for (a) $Lx = 8\pi$ and (b) $Lx = 20\pi$; time variation of energy density parts at $Re = 4500$ for (c) $Lx = 8\pi$ and (d) $Lx = 20\pi$.

3.1. *Nonlinear edge states*

After Orr amplification, nonlinear interactions are evoked to defeat the decay of the disturbance, then the edge state could be touched for fully energy-conserved nonlinear interactions (Camobreco, Pothérat & Sheard 2023; Huang *et al.* 2024). The time evolution of the optimal disturbance energy is shown in figure 1. The nonlinear optimal perturbations for sufficiently long channels could be identified (Huang *et al.* 2024) and minimal seeds are input as an initial condition for DNS. The initial perturbation of 2-D flow is amplified rapidly and decreased before saturated nonlinear interactions related to the energy plateau are evoked for different Re, as shown in figures 1(a) and 1(b). The transitional flow is triggered after a long period of saturated nonlinear interactions. The overshoots of disturbance energy are observed within a short time period less than 40 before the nonlinear edge state is approached in the disturbance energy variation, which is consistent with the previous study in the 3-D plane Couette flow (Duguet *et al.* 2010). Furthermore, the time variations of E_u and E_v are shown in figures 1(c) and 1(d). Interestingly, E_u is much larger than E_v for the minimal seed, while they are comparable for the edge state. This means that E_v experiences a larger energy gain than E_u as the minimal seed approaches the edge state, which is qualitatively in agreement with the theoretical analysis. Recall that the initial disturbance is the wall mode with the relation $E_u \sim Re^{2/3} E_v$ in the theoretical analysis, and the disturbance energies are comparable at the nonlinear edge state. Consequently, E_v is assumed to be amplified by Re^2 in the theoretical analysis based on the OS equation (2.9). Therefore, E_u initially is much larger than E_v, and E_v has

https://doi.org/10.1017/jfm.2025.10966 Published online by Cambridge University Press

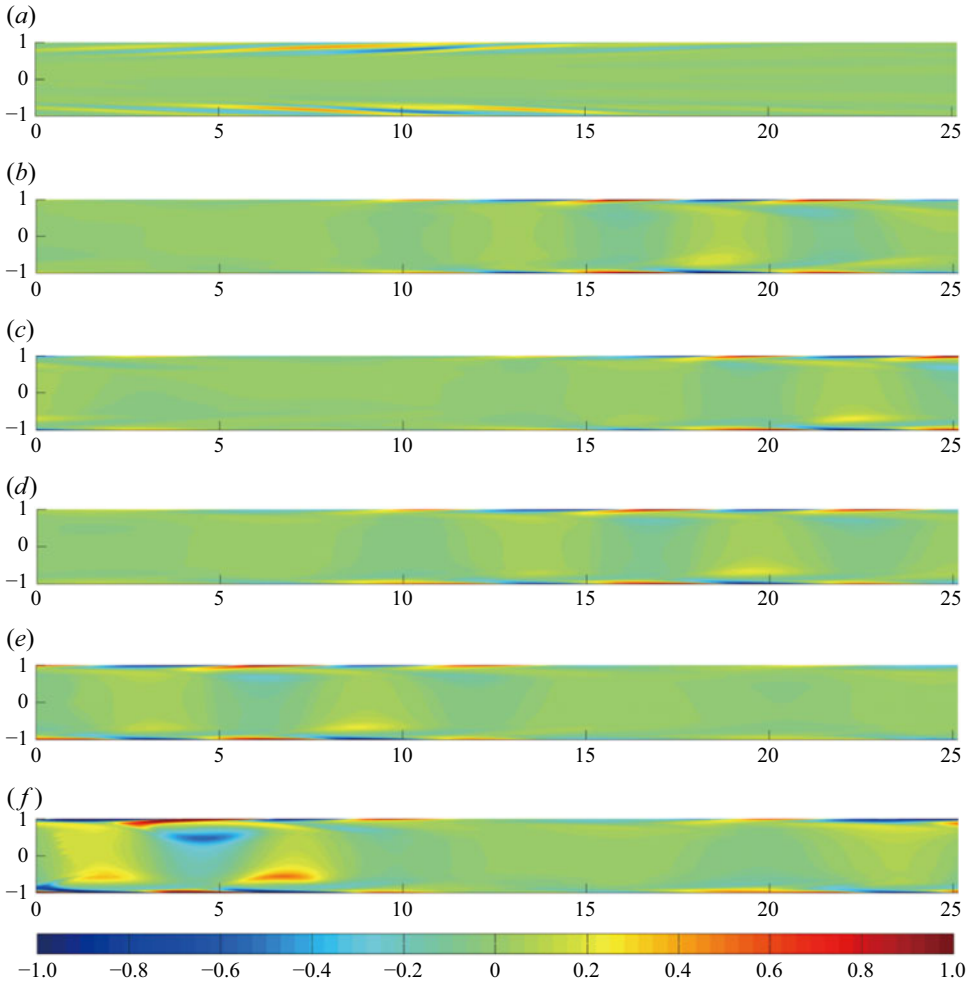


Figure 2. The evolution of minimal seed is represented by vorticity at different time instants for $Lx = 8\pi$ and $Re = 4500$. The time instants for snapshots $(a)-(f)$ are $t = 0$, 20, 30, 400, 700 and 1000, respectively.

amplification much larger than E_u. The numerical results as shown in figures 1(c) and 1(d) are consistent with the theoretical analysis.

The evolution of the minimal seeds and the coherent structures by the nonlinear non-modal instability analysis is shown in figure 2 for $Lx = 8\pi$. The localized optimal disturbances with three pairs of vortices are wall modes and are located against the mean shear near the channel walls. It is amplified by the Orr mechanism to obey the mean shear from figure 2(a) to figure 2(b) and reach the nonlinear edge state with a long time period from figure 2(c–e), before reaching the transitional state shown in figure 2(f). The fluid structures of the nonlinear travelling waves are packed and predominated approximately half of the channel and are consistent with observations (Jiménez 1990; Huang *et al.* 2024). It should be noted that the streamwise localized nonlinear optimal disturbance with three pairs of vortices is also found in the long channel $Lx = 20\pi$, which is not presented here since it was shown in figure 3 in Huang *et al.* (2024). Although the energy density is different for the two channels, the total disturbance energies are very close because of the streamwise localization of the nonlinear optimal disturbance. The nonlinear optimal

https://doi.org/10.1017/jfm.2025.10966 Published online by Cambridge University Press

Energies	Prediction	$Lx = 8\pi$	$Lx = 20\pi$	Conclusion
E_{0ms}	11/3 (≈3.67)	3.71	3.62	3.67 ± 0.05
E_{ums}	11/3 (≈3.67)	3.70	3.61	3.67 ± 0.06
E_{vms}	13/3 (≈4.33)	4.37	4.30	4.33 ± 0.04
E_{0es}	7/3 (≈2.33)	2.35	2.36	2.33 ± 0.03
E_{ues}	7/3 (≈2.33)	2.29	2.32	2.33 ± 0.04
E_{ves}	7/3 (≈2.33)	2.46	2.43	2.33 ± 0.13

Table 1. Comparisons of theoretical and numerical threshold κ for the energy parts. The subscript *ms* denotes minimal seed and *es* denotes edge state.

disturbance might be confined in a small channel and the nonlinear interactions could be limited. Therefore, in this study, long enough channels offering streamwise localized nonlinear optimal disturbance are chosen to validate our theoretical predictions.

3.2. *Thresholds for subcritical transition*

Theoretical analysis shows that the magnitudes of disturbances of u and v are approximately $O(Re^{-7/6})$ around the edge state for the minimal seeds. Recall that the amplification of $O(Re)$ for velocity v by the Orr mechanism, the optimal wall mode disturbance for v should be $O(Re^{-13/6})$. It should be noted that the optimal disturbance obeys the wall mode scaling rules, the disturbance energy of E_u is approximately $O(Re^{2/3})$ times E_v. Therefore, the thresholds that reveal the full processes of the most dangerous and efficient subcritical transitional flow in energy form are listed in table 1, $E_{vms} \sim Re^{-13/3}$, $E_{ums} \sim Re^{-11/3}$ and $E_{0ms} = (E_{ums} + E_{vms}) \sim Re^{-11/3}$, since the energy along the edge state is $E_{es} \sim Re^{-7/3}$.

Huang *et al.* (2024) found that the energy of the initial linear optimal disturbances would be larger than the energy of their edge state for 2-D plane Poiseuille flow. It means that the linear optimal disturbances are not good candidates for theoretical validations. The minimal seed represents the most dangerous disturbance that triggers the subcritical transition (Kerswell 2018). Therefore, the numerical scaling law of the threshold obtained directly from the minimal seed is perfect to verify these predictions. The energy density and the energy parts of the minimal seed are shown in figures 3(*a*) and 3(*b*). The energy threshold decays with the Reynolds number as $Re^{-3.71}$ and $Re^{-3.62}$ for $Lx = 8\pi$ and $Lx = 20\pi$, respectively. The numerical scaling laws agree well with the theoretical predicted value $-11/3$. Interestingly, the initial energy of the streamwise velocity E_{ums} is dominant and close to the total perturbation energy E_{0ms}, while the initial energy of the vertical velocity E_{vms} is much smaller. More precisely, E_{ums} scales as $Re^{-3.70}$ and $Re^{-3.61}$ for $Lx = 8\pi$ and $Lx = 20\pi$, respectively; while E_{vms} scales as $Re^{-4.37}$ and $Re^{-4.30}$ for $Lx = 8\pi$ and $Lx = 20\pi$, respectively. Furthermore, it should be noted that E_{ums} is approximately $Re^{0.67}$ and $Re^{0.69}$ times E_{vms} for $Lx = 8\pi$ and $Lx = 20\pi$, respectively. The numerical results are in perfect agreement with the theoretical analysis of wall mode disturbances.

The numerical results show that the target times are long enough to capture the long-sustained nonlinear edge state and transition thresholds for different channel lengths. This indicates that the theoretical predictions of the disturbance energy of the edge state should be correct. Since the energy varies very slowly along the saturated nonlinear edge state, the naïve and robust mean energy densities are adopted to observe the scaling laws. To measure the disturbance energy along the edge state, the disturbance energy is averaged from $t = 400$ to 700 for $Lx = 8\pi$, while the energy is averaged from $t = 400$

https://doi.org/10.1017/jfm.2025.10966 Published online by Cambridge University Press

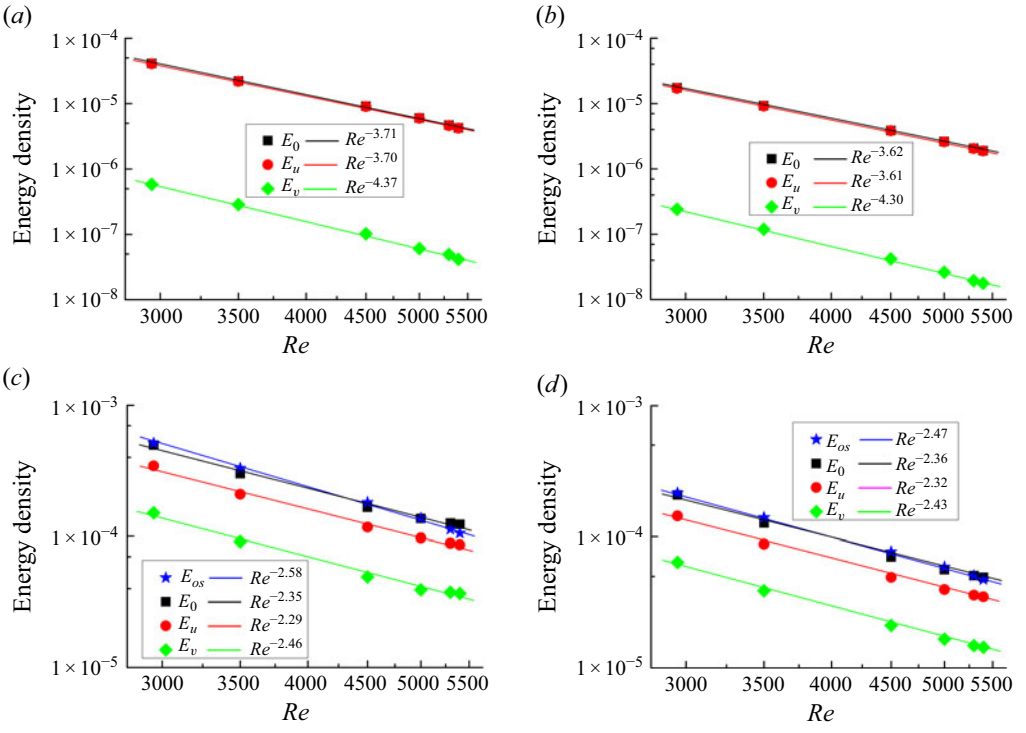


Figure 3. The scalings of disturbance energy threshold of minimal seed with respect to Re in log–log scale for (*a*) $Lx = 8\pi$ and (*b*) $Lx = 20\pi$; the scalings of energy of overshoot and edge state with respect to Re in log–log scale for (*c*) $Lx = 8\pi$ and (*d*) $Lx = 20\pi$.

to 1400 for $Lx = 20\pi$. Therefore, the energy and energy parts of the edge state with saturated nonlinear interactions near the transition point are also summarized and shown in figures 3(*c*) and 3(*d*). More interestingly and importantly, E_{0ms} and E_{ums} along the nonlinear edge state scale with Re as $Re^{-2.35}$ and $Re^{-2.29}$, respectively, for $Lx = 8\pi$; while E_{0ms} and E_{ums} scale with Re as $Re^{-2.36}$ and $Re^{-2.32}$, respectively, for $Lx = 20\pi$. All the scaling laws are very close to the theoretical prediction $Re^{-2.33}$ along the edge state, since E_{vms} scales with Re as $Re^{-2.46}$ for $Lx = 8\pi$ and $Re^{-2.43}$ for $Lx = 20\pi$, which are slightly smaller than the prediction.

The disturbance energy of the overshoot E_{os} with respect to Re is also presented in figures 3(*c*) and 3(*d*). We can see that the disturbance energy overshoots E_{os} are very close to the E_{0ms} along the edge state. More specifically, E_{os} is slightly higher than E_{0ms} for small Re, while E_{os} is slightly lower than E_{0ms} for large Re. Therefore, the scale of E_{os} is sharper than that of E_{0ms}, and E_{os} scales $Re^{-2.58}$ and $Re^{-2.47}$ for $Lx = 8\pi$ and $Lx = 20\pi$, respectively. In this study, we focus on saturated nonlinear interactions along the nonlinear edge state with a sufficiently long time period both theoretically and numerically. Therefore, the time-averaged disturbance energy along the nonlinear edge state could be better to show the nonlinear interactions, while the overshoots might not reflect the full information of the nonlinear interactions.

The disturbance energy should be approximately $Re^{-7/3}$ to sustain the nonlinear edge state in 2-D plane Poiseuille flow, which is similar to the results of the 3-D plane Couette flow since the streamwise rolls of approximately Re^{-2} are needed to sustain the edge state with streaks for the coherent states of the lower branch (Wang, Gibson & Waleffe 2007).

https://doi.org/10.1017/jfm.2025.10966 Published online by Cambridge University Press

It is interesting that the required disturbance energies are close for different shear flows, which indicates that the present asymptotic analysis in 2-D plane Poiseuille flow might be helpful for 3-D shear flows. However, the total disturbance energies to sustain the edge state before triggering the subcritical transition are quite different. For the 2-D plane Poiseuille flow, the streamwise and wall-normal disturbance energies should be approximately $Re^{-7/3}$, and the transitional threshold is approximately $Re^{-11/3}$ based on the wall mode disturbance (Huang *et al.* 2024). However, for the 3-D plane Couette flow, the streamwise rolls of Re^{-2} are needed to sustain the streamwise streaks of Re^{0}, and the transitional threshold would be Re^{-2}, which is consistent with the results of the linear optimal disturbance (Duguet *et al.* 2010). Nevertheless, the results show that the proposed mechanism and theoretical framework to quantify the subcritical transition thresholds are correct in 2-D plane Poiseuille flow, and it might be helpful to estimate the nonlinear transition thresholds for the 3-D plane Couette flow.

4. Discussions and conclusions

We have introduced an innovative theory for determining the thresholds of subcritical transitional flow, based on a proposed self-consistent theoretical framework that integrates asymptotic analysis, transient growth and nonlinear non-modal stability analysis theories. The transition scenarios are elucidated by emphasizing the evolution of the most efficient disturbances along the edge state, which separates the attractors of the laminar and turbulent boundary basins. The optimal disturbance experiences Orr amplification, progressing into the edge state for a sufficiently long period, before the unstable manifold near the transition point is attracted by the turbulent attractor. Consequently, the transition threshold is quantified through the estimation of the magnitude in proximity to the transition point on the edge state, in addition to the linear Orr amplification.

The threshold of subcritical transitional flow in 2-D plane Poiseuille flow is chosen to illustrate the theory. The inner flow with the right scaling could be affected by the interactions of the nonlinear terms, and the matched boundary condition for the inner flow is focused to induce possible instability instead of just considering the magnitude. Therefore, the transition threshold is predicted to be $O(Re^{-7/6})$ for the magnitude or $O(Re^{-7/3})$ for the disturbance energy E_{es} along with the edge state. Thus, the disturbance energy threshold requires $O(Re^{-13/3})$ for E_v and $O(Re^{-11/3})$ for E_u for the initial optimal disturbance, which is predicted by the wall mode scaling (Lin 1944; Chapman 2002) and the continuity equation. We confirmed the mechanism and theory precisely by numerical experiments based on DNS. The minimal seeds of different channels and different target times are numerically captured and show that the threshold of subcritical transitional flow is $E_{ms} \sim Re^{-3.67\pm0.05}$ since $E_u \sim Re^{-3.67\pm0.06}$ and $E_v \sim Re^{-4.33\pm0.04}$. All stages of the subcritical transitional flow are quantitatively consistent with the theoretical analysis. The theoretical framework addresses the determination of subcritical transitional thresholds in 2-D plane Poiseuille flow, and mutually validated in conjunction with the nonlinear non-modal stability analysis based on DNS.

It is interesting that the required disturbance energy is approximately $Re^{-7/3}$ for the nonlinear edge state in the 2-D plane Poiseuille flow, which is very close to the required streamwise rolls of approximately Re^{-2} for the lower branch coherent states in the 3-D plane Couette flow (Wang *et al.* 2007). Although they result in different transitional thresholds for minimal seeds, the idea of the present asymptotic analysis to quantify the required nonlinear disturbance energy along the edge state might be generic and could be extended to 3-D plane shear flows. Recall that the wall mode disturbance has been observed (Huang *et al.* 2024) for the 2-D plane Poiseuille flow and was used

https://doi.org/10.1017/jfm.2025.10966 Published online by Cambridge University Press

to construct the theoretical framework to predict the transition thresholds. The energy-conserved nonlinear interactions along the edge state are another key feature in the analysis. Moreover, according to Schmid & Henningson (2001) and Chapman (2002), the wall mode disturbances of the 3-D plane Couette flow are very important for transient growth, and the disturbance energy plateau is maintained along the nonlinear edge state (Rabin *et al.* 2012). Therefore, the theoretical analysis proposed in this study could be performed for the realistic 3-D plane Couette flow in the near future. For 3-D plane Poiseuille flow, both the wall and centre modes would result in streamwise streaks with considerable transient growth (Chapman 2002). Nevertheless, the present theory could also be extended to 3-D plane Poiseuille flow. Moreover, the theoretical and numerical results would be validated by the experimental observations with sufficiently long inlet for 3-D plane Poiseuille flows (Nishioka & Ichikawa 1975; Elofsson & Alfredsson 1998; Philip, Svizher & Cohen 2007; Lemoult *et al.* 2012).

Funding. The research was supported by the National Natural Science Foundation of China grants nos. 12102331, 52130603 and 52206053.

Declaration of interests. The authors report no conflict of interest.

References

Avila, K., Moxey, D., Lozar, A.D., Avila, M., Barkley, D. & Hof, B. 2011 The onset of turbulence in pipe flow. *Science* **333** (6039), 192–196.

Barkley, D., Song, B., Mukund, V., Lemoult, G., Avila, M. & Hof, B. 2015 The rise of fully turbulent flow. *Nature* **526** (7574), 550–553.

Bedrossian, J., Germain, P. & Masmoudi, N. 2015 On the stability threshold for the 3D Couette flow in sobolev regularity. *Ann. Math.* **185** (2), 541–608.

Bedrossian, J., Germain, P. & Masmoudi, N. 2019 Stability of the Couette flow at high Reynolds number in 2D and 3D. *B. Am. Math. Soc.* **56**, 373–414.

Boffetta, G. & Ecke, R.E. 2012 Two-dimensional turbulence. *Annu. Rev. Fluid Mech.* **44**, 427–451.

Camobreco, C.J., Pothérat, A. & Sheard, G.J. 2023 Subcritical transition to turbulence in quasi-two-dimensional shear flows. *J. Fluid Mech.* **963**, R2.

Camobreco, C.J., Pothérat, A. & Sheard, G.J. 2020 Transition to turbulence in quasi-two-dimensional mhd flow driven by lateral walls. *Phys. Rev. Fluids* **5** (11), 113902.

Chapman, S.J. 2002 Subcritical transition in channel flows. *J. Fluid Mech.* **451**, 35–97.

Del Zotto, A. 2023 Enhanced dissipation and transition threshold for the Poiseuille flow in a periodic strip. *SIAM J. Math. Anal.* **55** (5), 4410–4424.

Ding, S. & Lin, Z. 2022 Enhanced dissipation and transition threshold for the 2-D plane Poiseuille flow via resolvent estimate. *J. Differ. Equat.* **332**, 404–439.

Duguet, Y., Brandt, L. & Larsson, B.R.J. 2010 Scaling of the turbulence transition threshold in a pipe. *Phys. Rev. E.* **82**, 026316.

Duguet, Y., Monokrousos, L., Brandt, L. & Henningson, D.S. 2013 Minimal transition thresholds in plane Couette flow. *Phys. Fluids* **25**, 084103.

Elofsson, P.A. & Alfredsson, P.H. 1998 An experimental study of oblique transition in plane Poiseuille flow. *J. Fluid Mech.* **358**, 177–202.

Farano, M., Cherubini, S., Robinet, J.C. & Palma, P.D. 2015 Hairpin-like optimal perturbations in plane Poiseuille flow. *J. Fluid Mech.* **775**, R2.

Gustavsson, L.H. 1991 Energy growth of 3-d disturbances in plane Poiseuille flow. *J. Fluid Mech.* **224**, 241–260.

Hagan, J. & Priede, J. 2015 Two-dimensional nonlinear travelling waves in magnetohydrodynamic channel flow. *J. Fluid Mech.* **2760**, 387–406.

Hof, B., Doorne, C.W.H.V., Westerweel, J., Nieuwstadt, F.T.M., Faisst, H., Eckhardt, B., Wedin, H., Kerswell, R.R. & Waleffe, F. 2004 Experimental observation of nonlinear traveling waves in turbulent pipe flow. *Science* **305** (5690), 1594–1598.

Huang, Z., Gao, R., Gao, Y.Y. & Xi, G. 2024 Subcritical transitional flow in two-dimensional plane Poiseuille flow. *J. Fluid Mech.* **994**, A6.

https://doi.org/10.1017/jfm.2025.10966 Published online by Cambridge University Press

HUANG, Z. & HACK, M.J.P. 2020 A variational framework for computing nonlinear optimal disturbances in compressible flows. *J. Fluid Mech.* **894**, A5.
JIMÉNEZ, J. 1990 Transition to turbulence in two-dimensional Poiseuille flow. *J. Fluid Mech.* **218**, 265–297.
KERSWELL, R.R. 2018 Nonlinear nonmodal stability theory. *Annu. Rev. Fluid Mech.* **50**, 319–345.
LEMOULT, G., AIDER, J.L. & WESFREID, J.E. 2012 Experimental scaling law for the subcritical transition to turbulence in plane Poiseuille flow. *Phys. Rev. E.* **85**, 025303.
LIN, C.C. 1944 On the development of turbulence. PhD thesis, California Institute of Technology.
MARENSI, E., YALNIZ, G. & HOF, B. 2023 Dynamics and proliferation of turbulent stripes in plane-Poiseuille and plane-Couette flows. *J. Fluid Mech.* **974**, A21.
MONOKROUSOS, A., BOTTARO, A., BRANDT, L., VITA, A.D. & HENNINGSON, D.S. 2011 Nonequilibrium thermodynamics and the optimal path to turbulence in shear flows. *Phys. Rev. Lett.* **106** (13), 134502.
NISHI, M., UNSAL, B., DURST, F. & BISWAS, G.2008 Laminar-to-turbulent transition of pipe flows through puffs and slugs. *J. Fluid Mech.* **614**, 425–446.
NISHIOKA, M. & ICHIKAWA, Y. 1975 An experimental investigation of the stability of plane Poiseuille flow. *J. Fluid Mech.* **72** (4), 731–751.
ORR, W.M.F. 1907 The stability or instability of the steady motions of a perfect liquid and of a viscous liquid. Part i: a perfect liquid. *Proc. R. Irish Acad. A* **27**, 9–68.
ORSZAG, S.A. 1971 Accurate solution of the Orr–Sommerfeld stability equation. *J. Fluid Mech.* **50** (4), 689–703.
ORSZAG, S.A. & PATERA, A.T. 1980 Subcritical transition to turbulence in plane channel flows. *Phys. Rev. Lett.* **45** (12), 989–993.
PARENTE, E., ROBINET, J.-C., DE PALMA, P. & CHERUBINI, S. 2022 Minimal energy thresholds for sustained turbulent bands in channel flow. *J. Fluid Mech.* **942**, A18.
PHILIP, J., SVIZHER, A. & COHEN, J. 2007 Scaling law for a subcritical transition in plane Poiseuille flow. *Phys. Rev. Lett.* **98**, 154502.
PRINGLE, C.C.T. & KERSWELL, R.R. 2010 Using nonlinear transient growth to construct the minimal seed for shear flow turbulence. *Phys. Rev. Lett.* **105** (15), 154502.
PRINGLE, C.C.T., WILLIS, A.P. & KERSWELL, R.R. 2012 Minimal seeds for shear flow turbulence: using nonlinear transient growth to touch the edge of chaos. *J. Fluid Mech.* **702**, 415–443.
RABIN, S.M.E., CAULFIELD, C.P. & KERSWELL, R.R. 2012 Triggering turbulence efficiently in plane Couette flow. *J. Fluid Mech.* **712**, 244–272.
REDDY, S.C., SCHMID, P.J., BAGGETT, J.S. & HENNINGSON, D.S. 1998 On stability of streamwise streaks and transition thresholds in plane channel flows. *J. Fluid Mech.* **365**, 269–303.
REYNOLDS, O. 1883 An experimental investigation of the circumstances which determine whether the motion of water shall be direct or sinuous, and of the law of resistance in parallel channels. *Phil. Trans. R. Soc. Lond.* **35**, 84–99.
SCHMID, P.J. & HENNINGSON, D.S. 2001 *Stability and Transition in Shear Flows*. Springer.
SCHMID, P.J. 2007 Nonmodal stability theory. *Annu. Rev. Fluid Mech.* **39**, 129–162.
SULPIZIO, J.A., ELLA, L., ROZEN, A., BIRKBECK, J., PERELL, D.J., DUTTA, D., BEN-SHALOM, M., TANIGUCHI, T., WATANABE, K. & HOLDER, T. 2019 Visualizing Poiseuille flow of hydrodynamic electrons. *Nature* **576** (7785), 75–79.
TAYLOR, J.R. 2008 Numerical simulations of the stratified oceanic bottom boundary layer. PhD thesis, University of California.
TREFETHEN, L.N., CHAPMAN, S.J., HENNINGSON, D.S., MESEGUER, A., MULLIN, T. & NIEUWSTADT, F.T.M. 2000 Threshold amplitudes for transition to turbulence in a pipe. *Tech. Rep.* 00/17. Num. Anal. Group Report NA. 00/17. Oxford Univ.
TREFETHEN, L.N., TREFETHEN, A.E., REDDY, S.C. & DRISCOLL, T.A. 1993 Hydrodynamic stability without eigenvalues. *Science* **261** (5121), 578–584.
WANG, J., GIBSON, J. & WALEFFE, F. 2007 Lower branch coherent states in shear flows: transition and control. *Phys. Rev. Lett.* **98**, 204501.
WILLIS, A.P. & KERSWELL, R.R. 2009 Turbulent dynamics of pipe flow captured in a reduced model: puff relaminarization and localized 'edge' states. *J. Fluid Mech.* **619**, 213–233.

https://doi.org/10.1017/jfm.2025.10966 Published online by Cambridge University Press